Mon. Not. R. Astron. Soc. **000**, 1–14 (2008) Printed 30 May 2008 (MN LATEX style file v2.2)

The pulsating hot subdwarf Balloon 090100001: the results of 2005 multisite campaign

A. Baran[1,2⋆], R. Oreiro[3,4], A. Pigulski[5], F. Pérez[3,6], A. Ulla[7], M.D. Reed[8], C. Rodríguez-López[9], P. Moskalik[10], S.-L. Kim[11], W-P. Chen[12], R. Crowe[13], M. Siwak[14], L. Armendarez[13], P.M. Binder[13], K.-J. Choo[11], A. Dye[13], J.R. Eggen[8], R. Garrido[9], J.M. Gonzáles[3], S.L. Harms[8], F.-Y. Huang[12], D. Kozieł[14], H.-T. Lee[12], L. Fox Machado[3], T. Monserrat[3], J. Stevick[13], S. Stewart[13], D. Terry[13], A.-Y. Zhou[8,15], S. Zoła[1,14]

[1]*Cracow Pedagogical University, ul. Podchorążych 2, 30 – 084 Kraków, Poland*
[2]*Toruń Centre for Astronomy, ul. Gagarina 11, Toruń, Poland*
[3]*Instituto de Astrofísica de Canarias, 38200 La Laguna, Spain*
[4]*Institue of Astronomy, Katholieke Universiteit Leuven, Celestijnenlaan 200D, 3001 Leuven, Belgium*
[5]*Instytut Astronomiczny Uniwersytetu Wrocławskiego, ul. Kopernika 11, 51 – 622 Wrocław, Poland*
[6]*Dpto. Astrofísica, Universidad de La Laguna, 38200 La Laguna, Spain*
[7]*Dpto. Física Aplicada, Universidade de Vigo, 36200 Vigo, Spain*
[8]*Department of Physics, Astronomy and Materials Science, Missouri State University, 901 S. National, Springfield, MO 65897, USA*
[9]*Instituto de Astrofísica de Andalucía – C.S.I.C., Camino Bajo de Huétor 50, E – 18008 Granada, Spain*
[10]*Copernicus Astronomical Centre, ul. Bartycka 18, 00-716 Warsaw, Poland*
[11]*Korea Astronomy and Space Science Institute, Daejeon 305-348, South Korea*
[12]*Institute of Astronomy, National Central University, Jhongli 32054, Taiwan*
[13]*Department of Physics and Astronomy, University of Hawaii – Hilo, 200 West Kawili Street, Hilo, Hawaii 96720-4091, USA*
[14]*Jagiellonian University, ul. Orla 171, 30-244 Kraków, Poland*
[15]*National Astronomical Observatories of the Chinese Academy of Sciences, Beijing 100012,P.R. China*

Accepted .... Received ....; in original form ....

ABSTRACT

We present the results of a multisite photometric campaign on the pulsating sdB star Balloon 090100001. The star is one of two known hybrid hot subdwarfs with both long- and short-period oscillations, theoretically atributed to g- and p-modes. The campaign involved eight telescopes with three obtaining $UBVR$ data, one Strömgren $uvby$ photometry, and one B-band data. The campaign covered 48 nights, providing a temporal resolution of 0.36 μHz with a detection threshold of about 0.2 mmag in B-filter data.

Balloon 090100001 has the richest pulsation spectrum of any known pulsating subdwarf B star and our analysis detected 114 frequencies including 97 independent and 17 combination ones. Most of the 24 g-mode frequencies are between 0.1 and 0.4 mHz. Of the remaining 73, presumably p-modes, 72 group into four distinct regions near 2.8, 3.8, 4.7 and 5.5 mHz. The density of frequencies requires that some modes must have degrees ℓ larger than 2. The largest amplitudes have the modes in the 2.8 mHz region. The strongest mode (f_1) is most likely radial while the remaining ones in this region form two nearly symmetric multiplets: a triplet and quintuplet, attributed to rotationally split ℓ = 1 and 2 modes, respectively. We find clear increases of splitting in both multiplets between the 2004 and 2005 observing campaigns, amounting to $\sim$15% on average. The observed splittings imply that the rotational rate in Bal09 depends on stellar latitude and is the fastest on the equator. We also speculate on the possible reasons of the changes of splitting. The only plausible explanation we find are torsional oscillations. This hypothesis, however, need to be verified in the future by detailed modeling. In this context, it is very important to monitoring the splittings on a longer time scale as their behaviour may help to explain this interesting phenomenon.

The amplitudes of almost all terms detected both in 2004 and 2005, were found to vary. This is evident even during one season; for example, amplitudes of modes f_8 and f_C were found to change by a factor of 2–3 within about 50 days during 2005.

We use a small grid of models to constrain the main mode (f_1), which most likely represents the radial fundamental pulsation. The groups of p-mode frequencies appear to lie in the vicinity of consecutive radial overtones, up to the third one. Despite the large number of g-mode frequencies observed, we failed to identify them, most likely because of the disruption of asymptotic behaviour by mode trapping. The observed frequencies were not, however, fully exploited in terms of seismic analysis which should be done in the future with a larger grid of reliable evolutionary models of hot subdwarfs.

Key words: oscillations – subdwarf – stars: individual: Balloon 090100001.

1 INTRODUCTION

Kilkenny et al. (1997) discovered the first group of B-type hot subdwarf (sdB) pulsators, which they termed EC 14026 after the prototype and are now designated as V 361 Hya stars, and referred to as sdBV stars. This discovery opened the possibility of constraining the insides of sdB stars through asteroseismology, which, in turn, may help to better understand their still controversial evolution. So far, about 40 class members have been found, with periods ranging from 60 to 600 s and typical amplitudes of 10 mmag, with some exceptions of higher amplitudes up to 60 mmag. Theoretical studies by Charpinet et al. (1997) demonstrated that their oscillations could be explained by acoustic (p-) modes of low degree, ℓ, and low radial orders, n, driven by an opacity bump caused by a local enhancement of iron-group elements.

In 2002 another class of pulsating sdB stars was found (Green et al. 2003). The new class is characterised by lower amplitudes (1 – 2 mmag) and longer periods ($\sim$1 hour). The new variable stars are referred to as long-period sdBs, or PG 1716 stars, after that prototype. Fontaine et al. (2003) determined that their variability could be explained in terms of high radial order gravity (g-) modes. The same κ mechanism that operates in V 361 Hya stars works also in PG 1716 stars although model unstable modes were at slightly lower effective temperatures than observed. Jeffery & Saio (2006), using OP opacity tables and considering an enhancement of both iron and nickel in the driving zone, were able to obtain unstable modes at the same effective temperatures as the observed ones. Additionally, their non-adiabatic analysis led to simultaneous instability of p- and g-modes, which can account for the two known hybrid sdB pulsators.

The two classes (V 361 Hya and PG 1716 stars) of pulsating sdBs have slightly different effective temperatures and surface gravities, the former being hotter and denser than the latter. Their pulsating behaviour resemble two other pairs of pulsating stars showing p- and g-modes: β Cephei and Slowly Pulsating B stars and δ Scuti and γ Doradus stars.

2 BALLOON 090100001

Balloon 090100001 (hereafter Bal 09) is one of the brightest pulsating sdB stars discovered to date. It was found to be an sdB star by Bixler et al. (1991), and a short-period pulsating sdB by Oreiro et al. (2004). It has relatively long periods and large amplitudes of oscillation, which makes this object an excellent candidate for follow-up photometry. Bal 09 was observed in a long-time base campaign independently by two of us, in August and September 2004 using the 60-cm telescope at Mt. Suhora Observatory (AB) and the 80-cm IAC80 telescope at Tenerife (RO). Four wide-band filters, $UBVR$, were used in the former (Baran et al. 2005, hereafter Bar05), while only B-filter data were obtained in the latter (Oreiro et al. 2005, hereafter Ore05). The use of a common filter allowed an analysis of the combined data, from which almost 50 frequencies were detected (Baran et al. 2006). These campaigns revealed a rich spectrum of frequencies clustering in groups within the p-mode domain, and having lower amplitudes as the frequency increases. A high-amplitude frequency ($\sim$ 60 mmag) dominates the spectrum, with an equally-spaced triplet nearby. Assuming that the triplet splitting is caused by rotation, a rotational period near 7 days was derived. Interestingly, variability near 4 mmag was also detected in the low-frequency region, which is typical for PG1716 stars. Thus, Bal 09 turned out to be a hybrid object and from the seismological point of view the star became very interesting. Bal 09 was the second hybrid sdB pulsator discovered, the first being HS 0702+6043 (Schuh et al. 2006), which shows a single frequency in the g-mode region.

3 2005 PHOTOMETRIC CAMPAIGN

Despite the frequency resolution achieved with the 2004 observations, the spectrum of Bal 09 suffered from strong aliasing, hindering a clear frequency identification at lower amplitudes. Closely-spaced frequencies and/or amplitude variability made the situation even worse.

In order to get through these problems, a multisite campaign was organized in the summer of 2005. It involved eight telescopes at different longitudes, and spanned almost two months (10th August – 27th September). All sites but one used CCD cameras with Johnson B filter (or very similar), although some of them performed multicolour photometry in $UBVR$ filters. Moreover, Strömgren $uvby$ photometry was acquired with a photoelectric photometer attached to the 90-cm telescope in Sierra Nevada Observatory. The log of observations, including sites, observers and other relevant information is given in Table 1.

3.1 Data reduction

Raw CCD images were calibrated in a standard way by removing instrumental effects using bias, dark and flat field images. Magnitudes of stars were extracted using aperture photometry, but by means of different reduction pipelines: data collected at IAC 80 (Tenerife) were reduced with the Real Time Photometry (RTP) software (Østensen 2000); IDL photometry packages were applied to the Lulin (Taiwan) data; photometry from Sobaeksan (Korea) and Mt. Lemmon (Arizona) were proccessed with IRAF routines, while other CCD data were reduced by means of the DAOPHOT package with a DAOGROW supplement (Stetson 1987, 1990). Photoelectric photometry from the four-channel photoelectric photometer attached to the 90-cm telescope in Sierra Nevada Observatory was corrected assuming constant extinction coefficients determined from a nearby non-variable star.

Differential photometry for all filters was obtained using the reference star GSC 02248.00063, the most suitable due to its location in the field of view and magnitude. However, as it is much cooler than Bal 09, all data were corrected for second-order extinction effects. If, after this step, the light curve still showed long-period variations (on time scales much longer than a few hours), a spline fit was applied and subtracted from the data to remove those trends. The resulting light curves, obtained for each site separately, were then shifted to the same mean, converted to relative flux and combined. A similar conversion to relative fluxes has been done for the 2004 data. Consequently, all amplitudes provided in this paper are given in the units of 1/1000 of the relative flux (mma). In Fig. 1, the entire B and bv averaged light curves are presented.

3.2 Reanalysis of the combined 2004 data

As previously described, two independent photometric data sets of Bal 09 were obtained in 2004. As our analysis of the 2005 campaign data revealed amplitude variations (see Section 3.3), we decided to combine the 2004 B-filter data and reanalyse them in the same way as the 2005 campaign data. The 2004 data of Bar05 are better distributed in time and cover longer time interval than those of Ore05, allowing for a better distinction of close frequencies. On

Table 1. Details on the 2005 campaign. UH stands for University of Hawaii at Hilo. Other observer's abbreviations correspond to initials of the co-authors.

Telescope	Filter	HJD start	HJD end	Nights	Hours	Observers
IAC Teide, 0.8 m	U	620.37	628.75	7	44.2	RO, JMGP, TM, LF
	B	593.54	628.75	18	115.2	
	V	620.37	628.75	7	44.2	
	R	620.37	628.75	7	44.1	
Mt. Suhora, 0.6 m	U	594.47	639.51	34	226.9	AB, MS, DK, SZ
	B	594.47	639.51	36	216.6	
	V	594.47	639.51	34	226.9	
	R	594.47	639.51	34	226.9	
Baker, 0.4 m	U	594.68	624.91	11	79.2	MR, AYZ, SH, JRE
	B	594.68	625.87	13	92.4	
	V	594.68	594.79	1	2.7	
	R	594.68	624.96	11	80.0	
Lulin, 1 m	B	609.01	613.13	5	21.9	WPC, HTL, FYH
Sobaeksan, 0.6 m	B	618.01	630.03	5	23.3	SLK, KJC
Mauna Kea, 0.6 m	B	621.87	631.02	7	36.7	AB, RC, UH students
Mt. Lemmon, 1 m	B	636.84	640.63	5	29.0	SLK, KJC
Sierra Nevada, 0.9 m	$uvby$	605.41	618.62	14	105.6	CRL, RG

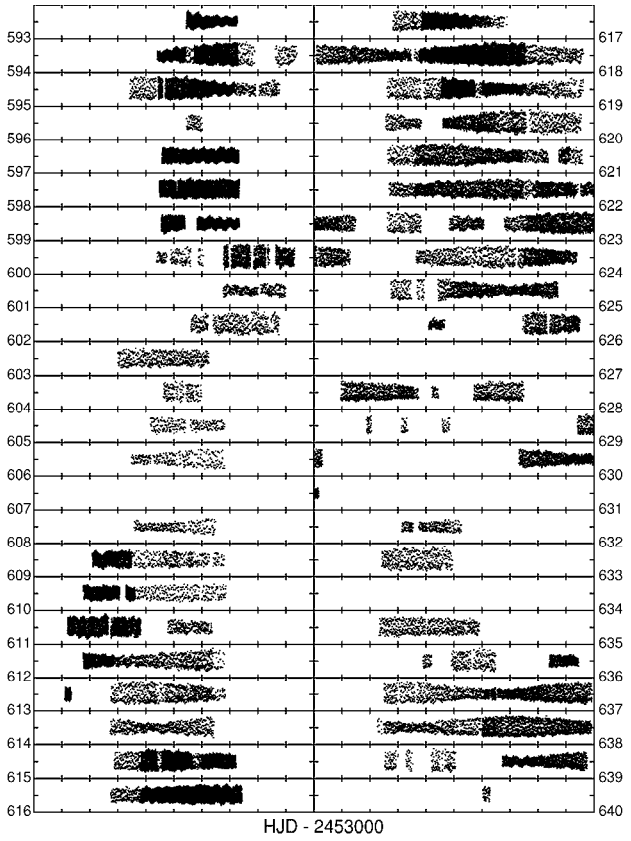

Figure 1. Observational data of Bal 09 in B and the average of b and v filters obtained in August and September 2005. Each panel covers one day and the numbers in the bottom left or right corners represent the three last integer digits of HJD for that panel. Note that consecutive days go vertically. The range in ordinate amounts to 240 mma.

the other hand, the data of Ore05 have better precision and were carried out with shorter time sampling. In order to balance the accuracy and resolution in the combined data, we decided to average three consecutive datapoints in the data of Ore05 before combining them together.

As will be described in Section 3.3 for the 2005 data, we analysed the 2004 data allowing for linear amplitude changes. The rates of these changes as well as the amplitudes and phases of all frequencies detected in the 2004 data are reported in Table 2. In total, we detected 56 frequencies of which 41 (12 in g-mode and 29 in p-mode regions) are independent and 15 are combination terms. In comparison to the analysis of Bar05, we found 26 more frequencies. This is mainly the consequence of lowering the detection level in the combined data. Of the 30 modes given by Bar05, we did not detect $f_{\rm E}$ and $f_{\rm H}$ in the g-mode region. This creates uncertainty as to whether they are intrinsic to Bal 09, but it is also possible that their amplitudes were changing quite fast, making them undetectable in the combined data (see for example Reed et al. 2007a). This is only possible if their amplitudes were very low at the beginning of the 2004 run when most of the Ore05 data were acquired. It is worth noting that the combined data revealed a fourth region of p-mode frequencies around 5.5 mHz. Frequencies in this region were reported by Ore05, but not detected by Bar05.

In Table 2 and throughout this paper, the notation of frequencies introduced by Bar05 is used and extended for new modes: frequencies in the g-mode region are annotated by letters while numbers are assigned to frequencies in the p-mode region. When a frequency was recovered at an alias frequency it is marked with '+' or '−'; for example $f_{12+} = f_{12} + 1\ \mathrm{d}^{-1}$ and $f_{12-} = f_{12} - 1\ \mathrm{d}^{-1}$. Table 2 of Bar05 indicated two possible aliases for a single frequency designated as f_{18}. We shall denote the two possibilities as $f_{18'}$ and $f_{18''}$, the frequency of the former being lower than the latter. According to this notation, the mode listed as f_{14} in Table 2 of Baran et al. (2008) should be designated as $f_{18''}$.

Table 2. A list of modes detected in the combined 2004 B filter data, while allowing for linear amplitude changes. Amplitudes and phases are given for HJD = 2 453 246. Numbers in brackets indicate the formal r.m.s. errors.

#	Frequency [mHz]	Ampl. A [mma]	dA/dt [mma/d]	Phase [rad]	#	Frequency [mHz]	Ampl. A [mma]	dA/dt [mma/d]	Phase [rad]
$f_{\rm I}$	0.229566(24)	0.57	+0.013	0.12(17)	f_{26}	3.822911(21)	0.70	−0.002	0.14(13)
$f_{\rm D}$	0.239973(07)	1.96	+0.010	5.80(05)					
$f_{\rm F}$	0.246315(22)	0.61	+0.003	2.64(15)	f_{11-}	4.633620(25)	0.57	0.000	1.26(17)
$f_{\rm A}$	0.272379(05)	2.75	−0.028	5.66(03)	f_{21}	4.644467(19)	1.14	−0.034	1.96(10)
$f_{\rm G}$	0.298886(19)	0.67	+0.003	6.23(13)	f_{27}	4.651166(25)	0.65	−0.005	2.20(15)
$f_{\rm C}$	0.325671(12)	1.25	+0.052	1.37(09)	f_{28}	4.655560(28)	0.80	−0.022	4.35(15)
$f_{\rm J}$	0.331210(16)	0.81	+0.007	1.42(11)	f_{29}	4.660107(22)	0.76	−0.009	2.70(13)
$f_{\rm B}$	0.365807(05)	2.66	−0.023	1.98(03)	f_{13}	4.661418(14)	1.07	+0.005	2.04(09)
$f_{\rm K}$	0.397189(26)	0.49	+0.011	0.48(20)	f_{30}	4.670320(17)	0.92	−0.002	4.24(11)
$f_{\rm L}$	0.631078(29)	0.44	+0.011	0.94(22)	f_{31}	4.676034(34)	0.65	−0.026	2.57(21)
$f_{\rm M}$	0.684352(21)	0.60	+0.002	4.77(14)	f_{12+}	4.680947(21)	0.78	−0.006	4.00(12)
$f_{\rm N}$	0.833085(25)	0.53	−0.006	4.84(17)					
					f_{32}	5.506010(28)	0.54	−0.013	1.16(18)
$f_8 - f_1$	0.968616	0.43	+0.001	5.21(20)	f_{33}	5.532958(21)	0.61	+0.009	3.86(15)
					f_{34}	5.553408(27)	0.48	−0.002	0.11(18)
$f_1 - f_{\rm B}$	2.441662	0.80	+0.001	1.11(11)	f_{35}	5.605820(28)	0.47	+0.002	4.13(19)
$f_1 - f_{\rm C}$	2.481799	0.43	+0.016	2.13(19)					
$f_1 - f_{\rm A}$	2.535091	0.41	+0.009	3.57(20)	$2f_1$	5.6149394	5.67	+0.003	3.874(16)
					$f_1 + f_2$	5.6307087	4.33	0.000	1.793(21)
f_1	2.8074697(02)	52.83	+0.058	2.6938(17)	$f_1 + f_3$	5.6322777	2.61	−0.022	0.94(04)
f_2	2.8232390(06)	20.39	+0.032	0.602(05)	$f_1 + f_4$	5.6338393	0.99	−0.003	4.10(10)
f_3	2.8248080(11)	12.13	−0.055	5.997(07)	$2f_2$	5.6464780	0.80	+0.001	5.75(12)
f_4	2.8263696(27)	5.09	−0.034	2.784(18)	$f_2 + f_3$	5.6480470	0.66	−0.002	4.87(14)
f_5	2.853958(08)	1.73	−0.001	5.19(5)	$f_1 + f_5$	5.661428	0.53	+0.002	0.44(17)
f_7	2.855710(10)	1.38	+0.009	2.27(7)					
f_6	2.858534(14)	1.15	−0.002	4.86(9)	$f_1 + f_8$	6.583556	0.55	−0.013	1.90(15)
f_{15}	3.763702(25)	0.61	+0.009	1.51(17)	$3f_1$	8.4224091	0.71	−0.010	5.37(12)
f_{23}	3.764802(30)	0.64	−0.003	2.54(16)	$2f_1 + f_2$	8.4381784	0.49	+0.005	2.83(18)
f_8	3.776086(05)	4.50	−0.045	0.914(24)	$2f_1 + f_3$	8.4397475	0.40	−0.009	2.05(21)
f_9	3.786724(13)	1.33	−0.007	2.51(08)					
f_{24}	3.791843(18)	1.00	−0.028	3.61(11)			$N_{\rm obs}$	12115	
f_{10}	3.795572(13)	1.05	+0.003	1.60(09)		Detection threshold [mma]		0.42	
$f_{18'}$	3.797813(23)	0.68	+0.007	4.94(16)		$\sigma_A, \sigma_{dA/dt}$ [mma, mma/d]		0.09	0.007
f_{25}	3.821887(28)	0.54	+0.014	1.22(20)		Residual S.Dev. [mma]		6.46	

3.3 Fourier analysis of the 2005 campaign data

Both the 2004 and 2005 data for Bal09 cover similar time intervals: nearly 40 days in 2004 and 50 days in 2005. The resulting resolution is therefore similar, but the improved duty cycle of the 2005 data resulted in a lower detection threshold and improved aliasing. Consequently, a larger number of frequencies was detected with the 2005 data.

Analysis for each filter of the 2005 data were done independently by means of the Fourier periodogram with consecutive prewhitening of detected frequencies. Due to the better time coverage, the largest number of frequencies were detected in the B-filter data even though some of them were easier to identify in data taken with other filters. Strömgren photometry was acquired at only one site, thus leading to a shorter list of frequencies. However, because in terms of time coverage, $UBVR$ and Strömgren $uvby$ data are complementary, we decided to combine them. In order to minimize the wavelength dependence of pulsation amplitudes, we combined the U data with the mean of the u and v (hereafter Uuv) data, the B data with the average of the v and b (hereafter Bvb) data, and the V and y (hereafter Vy) data. The spectral window for the Bvb data is shown in Fig. 2.

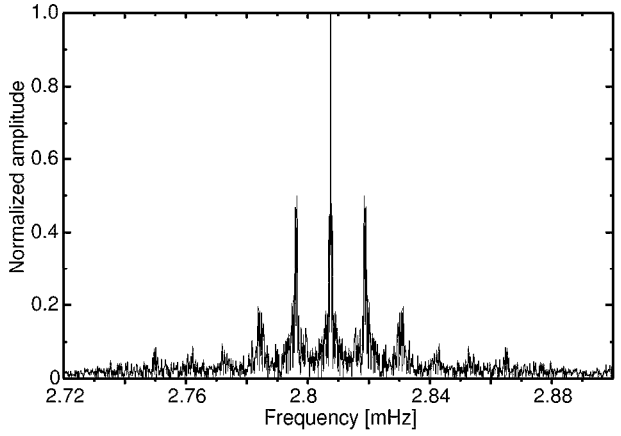

Figure 2. Spectral window for Bal 09 calculated from B and average of b and v data shifted to the frequency of the strongest mode.

In Fig. 3, the Fourier spectrum for Bvb data is shown. Since oscillations in Bal 09 are dominated by frequencies at 2.8 mHz,

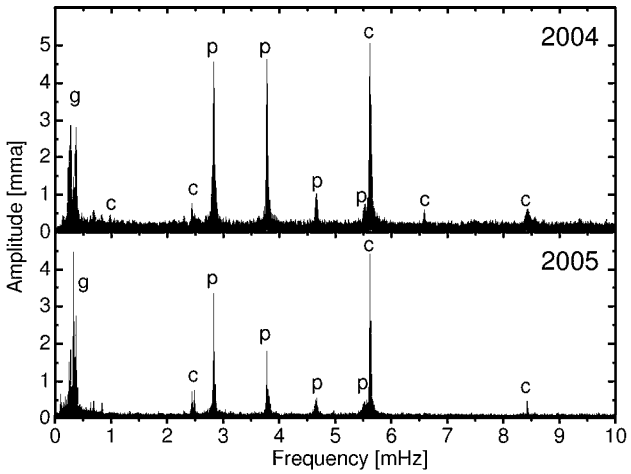

Figure 3. Fourier spectrum of the 2004 B (top) and 2005 Bvb data (bottom) after removing the three strongest frequencies near 2.8 mHz (f_1, f_2 and f_3, see Tables 2 and 3). Regions attributed to differing pulsation mechanisms (p- and g-modes), and their combinations are labeled with 'p', 'g', and 'c', respectively.

especially the strongest one with an amplitude near 50 mma, for clarity Fig. 3 presents the amplitude spectrum after removing three high-amplitude frequencies (f_1, f_2 and f_3). It can be seen that the same groups of frequencies are present that were in the 2004 campaign (Bar05, Ore05): the low-frequency region (mainly around 0.3 mHz), that of the dominant frequency (at 2.8 mHz) and three other groups (3.8, 4.7, 5.5 mHz) separated roughly by the same frequency distance (0.8–1.0 mHz). However their amplitudes have changed; the low-frequency pulsations, in particular, increased their amplitudes between 2004 and 2005 (Fig. 3). From the 2004 data Bar05 found only a weak evidence for amplitude variations, but those data were only sensitive to variations on a time scale of one or two weeks. However, amplitude variations are obvious between the 2004 and 2005 data sets. In order to infer the character of amplitude changes, we divided the 2005 Bvb data into 33 overlapping subsets. The consecutive subsets contain data covering time intervals of 10 days, from the beginning of each night. The results for the six strongest frequencies (f_1 through f_4, f_8, and f_C) are plotted in Fig. 4. Of these, only f_4 shows no amplitude variations.

For this reason, in the final analysis we allowed for linear amplitude changes. As can be seen from Fig. 4, this model is not always a good approximation of real changes. However, it is at least a reasonable choise which does not produce a large number of free parameters which need to be derived. The consecutive prewhitening in which linear amplitude changes were allowed led to a less noisy residual spectrum than in the case when amplitudes were assumed to be constant, particularly in the vicinity of the strongest frequencies.

The extraction of frequencies for the 2005 data was done independently for Uuv, Bvb, Vy and R data. For Uuv, Vy and R, the process was continued until all terms with signal-to-noise (S/N) above 4 were extracted. This was done in a typical way, i.e. by consecutive prewhitening and then non-linear improvement of frequencies, amplitudes and phases simultaneously for all previously detected terms. For the Bvb data, we used the same detection limit (S/N > 4), but the process neccessitated modification as the non-linear least-squares routines did not reach convergence once a large

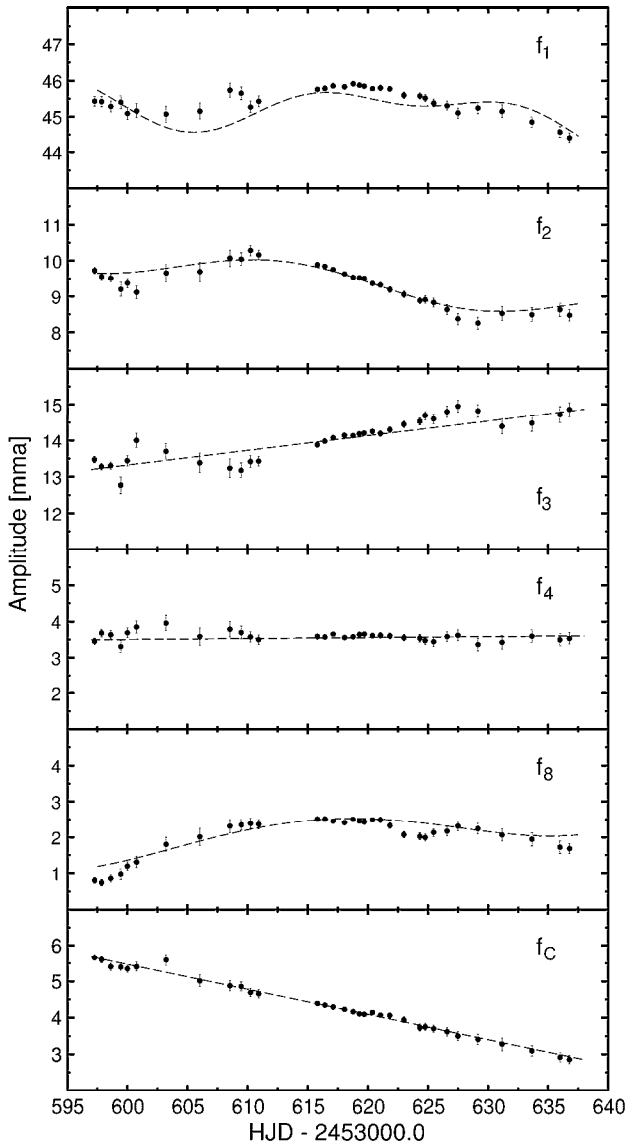

Figure 4. Amplitudes of the six strongest frequencies in Bal 09 for the 2005 Bvb data. From top to bottom the frequencies are f_1, f_2, f_3, f_4, f_8 and f_C (see Table 3). For f_3, f_4 and f_C the dashed lines correspond to changes calculated from the derived values of A and dA/dt (Table 3), for the remaining three frequencies they come from a more complicated model (see text for an explanation).

number of frequencies were fit. Therefore, we first obtained a preliminary solution which included all frequencies with amplitudes higher than 1 mma. Next, we took advantage of the fact that in Bal 09 frequencies appear in groups separated by several hundred microhertz. Thus we could safely assume that during iterations, frequencies from one group do not affect the solution for frequencies of the other groups. We obtained the final solution for Bvb data using six groups. In this process, we first subtracted frequencies from the other groups taken from the preliminary solution and used the residuals as a starting point for the extraction of frequencies in the considered group. Again, the detection limit was S/N = 4.

During the analysis of all four datasets we allowed for linear amplitude changes for the terms which had amplitudes at least ~3.5

Table 3. Modes detected in 2005 data in the Uuv, Bvb, Vy and R data. Numbers in parentheses indicate the r.m.s. errors. Phases and amplitudes are given for epoch HJD 2 453 615.

#	Mean freq.	Amplitude, A [mma], dA/dt [mma/d]				Phase [rad]			
	[mHz]	Uuv	Bvb	Vy	R	Uuv	Bvb	Vy	R
$f_{\rm O}$	0.096902(09)	...	0.70,−0.031	...	...	...	4.86(07)	...	
$f_{\rm P}$	0.139161(22)	...	...	0.77, —	...	...	...	1.15(13)	
$f_{\rm Q}$	0.142459(10)	...	0.59, —	...	...	...	3.37(07)	...	
$f_{\rm R}$	0.144996(22)	...	...	0.79, —	...	...	...	5.65(13)	
$f_{\rm S}$	0.169849(10)	...	0.58, —	...	...	...	4.09(07)	...	
$f_{\rm T}$	0.175656(08)	...	0.68, —	0.88, —	...	...	0.90(06)	0.56(12)	
$f_{\rm U}$	0.192869(21)	...	...	0.83, —	...	...	...	3.41(12)	
$f_{\rm V}$	0.198935(11)	...	0.54, —	...	...	...	5.89(08)	...	
$f_{\rm I}$	0.229549(09)	...	0.85,−0.027	...	0.49, —	...	5.01(06)	...	4.95(19)
$f_{\rm D}$	0.239971(07)	1.68, —	1.08,+0.019	0.99, —	0.85, —	5.81(08)	5.99(04)	5.98(10)	5.73(11)
$f_{\rm F}$	0.246301(05)	1.80, —	1.52,+0.018	1.66,−0.004	1.37, —	1.79(07)	1.613(27)	1.58(06)	1.57(07)
$f_{\rm A}$	0.272463(05)	1.67, —	1.72,−0.002	1.45, —	1.49, —	1.37(08)	1.473(23)	1.58(07)	1.57(07)
$f_{\rm W}$	0.29380(03)	...	...	...	0.52, —	...	...	...	2.20(18)
$f_{\rm G+}$	0.310575(11)	0.85, —	0.72,−0.008	0.56, —	0.58, —	4.57(15)	4.66(06)	4.70(18)	4.88(16)
$f_{\rm C}$	0.3256089(18)	4.84,−0.077	4.44,−0.069	3.82,−0.019	3.71,−0.053	4.590(27)	4.609(10)	4.609(27)	4.613(26)
$f_{\rm J}$	0.331182(10)	0.71, —	0.75,−0.002	0.79, —	0.61, —	0.87(18)	6.19(05)	0.58(13)	6.25(15)
$f_{\rm B}$	0.365805(03)	3.36,−0.014	2.65,−0.013	2.52,−0.006	2.64,+0.002	6.20(04)	6.180(15)	0.06(04)	6.22(04)
$f_{\rm K}$	0.397232(09)	0.67, —	0.84, 0.000	0.97, —	0.56, —	3.01(19)	2.52(05)	2.63(11)	2.52(17)
$f_{\rm L}$	0.630740(15)	...	0.42, —	0.49, —	...	...	1.36(09)	1.64(21)	...
$f_{\rm M}$	0.684405(14)	...	0.47, —	0.56, —	0.38, —	...	5.02(08)	4.90(18)	4.91(25)
$f_{\rm N}$	0.833090(14)	0.59, —	0.43, —	...	...	4.67(22)	4.77(09)	...	...
$f_{\rm X}$	1.845938(27)	...	0.20, —	...	...	...	4.48(19)	...	...
$f_{\rm Y}$	1.95968(04)	0.59, —	...	...	...	0.55(22)	...	...	...
$f_{\rm Z}$	2.296144(22)	...	0.25, —	...	...	...	4.23(15)	...	...
$f_1 - f_{\rm K}$	2.410232	...	0.22, —	...	...	...	3.68(18)	...	...
$f_1 - f_{\rm B}$	2.441659	0.86, —	0.69, —	0.51, —	0.47, —	6.06(14)	0.14(06)	6.23(18)	6.14(18)
$f_1 - f_{\rm C}$	2.4818552	0.81, —	0.77,−0.013	0.93, —	0.63, —	1.81(14)	1.98(05)	1.74(10)	1.78(14)
$f_3 - f_{\rm C}$	2.4992272	...	0.20, —	...	...	...	4.75(20)	...	...
$f_{\rm AA}$	2.707505(27)	...	0.20, —	...	...	...	3.34(19)	...	...
$2f_1 - f_3$	2.7900921	...	0.20, —	...	...	...	1.31(19)	...	...
f_1	2.80746412(16)	59.89,−0.048	45.48,−0.014	41.26,+0.019	40.08,−0.019	5.912(02)	5.934(01)	5.927(03)	5.934(03)
f_2	2.8230026(08)	11.16,−0.013	9.49,−0.033	8.61,−0.012	8.27,−0.019	0.638(12)	0.658(05)	0.653(12)	0.626(12)
f_3	2.8248361(06)	17.33,+0.029	13.93,+0.041	13.49,+0.015	12.88,+0.042	2.441(08)	2.457(03)	2.454(08)	2.428(08)
f_4	2.8265995(22)	4.11,+0.035	3.54,+0.003	3.16,+0.001	2.99,+0.005	2.16(03)	2.095(12)	2.01(04)	2.11(03)
f_5	2.853383(09)	1.06, —	0.92,−0.011	0.58, —	0.54, —	1.00(12)	0.95(05)	0.61(18)	1.13(18)
f_7	2.855571(10)	0.66, —	0.85,−0.008	0.82, —	0.68, —	5.16(20)	4.99(05)	5.00(13)	4.91(14)
f_{36}	2.857126(13)	1.05, —	0.59, —	0.69, —	0.59, —	0.33(13)	0.54(07)	0.73(15)	0.80(17)
f_6	2.858725(10)	0.91, —	0.88,−0.001	0.76, —	0.96, —	5.87(14)	5.74(05)	5.87(14)	5.67(10)
f_{37}	2.860737(16)	...	0.38, —	...	...	...	4.94(11)	...	...
f_{38}	3.036271(21)	...	0.28, —	...	...	...	4.96(13)	...	...
$f_1 + f_{\rm C}$	3.1330730	...	0.22, —	...	...	...	0.51(18)	...	...
$f_1 + f_{\rm B}$	3.173269	...	0.18, —	...	...	...	2.36(22)	...	...

times larger than the detection threshold, namely 2.0, 0.7, 1.6 and 1.5 mma, for Uuv, Bvb, Vy and R data, respectively. Fixing dA/dt = 0 for the low-amplitude modes allowed us to avoid problems with convergence which otherwise occured. However, this assumption does not affect the final quantity of frequencies detected.

The results of frequency extraction are presented in the following subsections and the full list is given in Table 3. The largest number of frequencies, 103, was detected in the Bvb data, as expected. In each of the remaining three datasets over thirty frequencies were detected. The total number of frequencies presented in Table 3 is 114, since some of them which were not detected in Bvb data were found in other datasets. Of these 114 frequencies, 17 are combination terms while the remaining 97 might represent independent modes.

The list of frequencies shown in Table 3 does not include several others which were very close to some large-amplitude terms, mainly f_1. These were unresolved or barely resolved and so we cannot exclude the possibility that they may be real frequencies. However the most plausible explanation is that they are artefacts caused by amplitude changes not accounted for using a constant dA/dt. This is shown in Fig. 4 for three frequencies detected in Bvb data (f_1, f_2 and f_8). The dashed lines reflect *apparent* ampli-

Table 3. continued.

#	Mean freq. [mHz]	Amplitude, A [mma], dA/dt [mma/d] Uuv	Bvb	Vy	R	Phase [rad] Uuv	Bvb	Vy	R
f_{39}	3.774190(15)	0.84, —	0.49, —	0.64, —	...	4.81(15)	3.96(09)	3.92(16)	...
f_8	3.776163(05)	2.30,−0.006	2.00,+0.023	2.26,−0.016	1.98,+0.008	4.04(06)	4.03(03)	3.95(05)	4.02(05)
f_{40}	3.777480(16)	...	0.46, —	...	...	...	1.49(10)	...	...
f_{41}	3.78451(03)	...	...	0.52, —	...	...	...	5.35(20)	...
f_{42}	3.784938(19)	...	0.37, —	...	...	...	2.71(11)	...	...
f_{43}	3.78533(03)	...	...	...	0.55, —	...	...	...	2.25(18)
$f_{44} = f_9$?	3.786291(17)	...	0.48, —	...	0.43, —	...	4.14(09)	...	4.21(23)
$f_{45} = f_9$?	3.787153(21)	...	0.37, —	...	...	...	4.18(14)	...	...
f_{46}	3.791291(15)	...	0.58, —	...	0.75, —	...	2.70(08)	...	2.47(14)
f_{24}	3.791581(12)	1.28, —	0.78,+0.030	0.74, —	0.57, —	0.91(10)	0.76(08)	1.10(14)	0.56(19)
f_{47}	3.792387(22)	...	0.36, —	...	...	...	0.62(13)	...	...
f_{48}	3.793419(20)	...	0.35, —	...	...	...	4.28(12)	...	...
f_{49}	3.796825(20)	0.61, —	0.39, —	...	...	5.45(21)	5.79(12)	...	...
f_{19}	3.80520(04)	...	...	0.51, —	...	...	...	1.09(20)	...
f_{20}	3.806574(22)	...	0.30, —	...	...	...	0.86(14)	...	...
f_{50}	3.807605(19)	...	0.36, —	...	...	...	5.11(12)	...	...
$f_{18''}$	3.808945(15)	...	0.44, —	...	...	...	4.45(09)	...	...
f_{51}	3.812194(17)	...	0.37, —	...	...	...	0.97(11)	...	...
$f_{52} = f_{26}$?	3.822485(17)	...	0.34, —	...	...	...	5.13(12)	...	...
f_{53}	3.824759(12)	...	0.55, —	...	0.48, —	...	1.71(07)	...	1.92(20)
f_{54}	3.829725(16)	...	0.42, —	...	...	...	2.17(12)	...	...
f_{55}	3.840824(23)	...	0.28, —	...	...	...	3.15(17)	...	...
f_{56}	4.636265(26)	...	0.25, —	...	...	...	3.45(17)	...	...
f_{57}	4.639892(15)	...	0.42, —	...	...	...	3.87(10)	...	...
f_{58}	4.641239(23)	...	0.36, —	...	0.42, —	...	3.37(12)	...	3.87(22)
f_{59}	4.641568(19)	...	0.47, —	0.59, —	...	...	3.17(10)	2.93(17)	...
f_{60}	4.642478(16)	...	0.49, —	...	...	...	2.91(10)	...	...
$f_{61} = f_{11}$?	4.645175(28)	...	0.27, —	...	...	...	1.59(17)	...	...
$f_{62} = f_{11}$?	4.645459(28)	...	0.33, —	...	...	...	5.54(13)	...	...
f_{63}	4.646299(16)	...	0.54, —	...	...	...	4.73(08)	...	...
f_{64}	4.647062(28)	...	0.28, —	...	...	...	1.77(18)	...	...
f_{65}	4.649385(22)	0.64, —	0.29, —	...	...	0.11(20)	0.16(15)	...	...
f_{66}	4.65294(04)	0.66, —	...	...	...	0.72(20)	...	...	...
f_{67}	4.653491(18)	...	0.44, —	...	...	...	4.11(12)	...	...
f_{68}	4.654759(20)	0.74, —	0.34, —	...	...	4.14(18)	3.71(13)	...	...
f_{12-}	4.658007(19)	...	0.41, —	...	...	...	4.32(12)	...	...
$f_{69} = f_{13}$?	4.66097(03)	...	...	0.53, —	...	...	...	4.14(19)	...
$f_{70} = f_{13}$?	4.661708(15)	...	0.40, —	...	...	...	2.02(10)	...	...
f_{71}	4.663070(25)	...	...	...	0.62, —	...	...	...	3.36(15)
f_{72}	4.665422(15)	...	0.55, —	0.46, —	...	...	4.36(08)	4.58(23)	...
f_{73}	4.666868(15)	0.64, —	0.58, —	0.37, —	0.55, —	5.96(20)	6.01(07)	6.10(28)	6.25(17)
f_{74}	4.668308(18)	...	0.37, —	...	...	...	4.22(11)	...	...
f_{75}	4.671570(23)	...	0.29, —	...	...	...	0.75(15)	...	...
f_{76}	4.674040(26)	...	0.24, —	...	...	...	1.98(17)	...	...
f_{77}	4.683263(23)	...	0.28, —	...	...	...	0.57(15)	...	...
f_{78}	4.708165(26)	...	0.21, —	...	...	...	0.25(18)	...	...

tude changes for a case when all 'ghost' terms were included in the solution. For the remaining three frequencies in Fig. 4, the constant rate of amplitude change model is good enough and therefore the 'ghost' terms did not appear close to them in the frequency spectrum.

As indicated by Fig. 4, the amplitudes of some terms change by a factor of two or more during 50 days (e.g. f_8 and f_C). As such, we cannot exclude the possibility that some nearby frequencies given in Table 3 are not independent but are artefacts caused by amplitude variations. Another problem is aliasing. This is particularly bad near 3.8, 4.7 and 5.5 mHz where low-amplitude frequencies are near to high-amplitude ones and the frequency density is very high. Again, it is possible that some of these frequencies are in error by 1 (sidereal day)$^{-1}$. Furthermore, some frequencies may also have changed. While these changes probably did not affect the analysis of any given year data, season-to-season changes are evident for some components of rotationally split multiplets, as discussed in Section 3.5. The changes of frequencies between 2004 and 2005 could be as large as 0.6 μHz (see Table 4), which may pose difficulties in cross-identifying frequencies detected in both seasons. That is why we provide multiple identifications and question marks for some of the frequencies in Table 3.

Table 3. continued.

#	Mean freq. [mHz]	Amplitude, A [mma], dA/dt [mma/d] Uuv	Bvb	Vy	R	Phase [rad] Uuv	Bvb	Vy	R
f_{79}	5.468920(22)	...	0.26, —	...	...	...	2.82(15)	...	...
f_{80}	5.476806(23)	...	0.25, —	...	...	...	4.63(16)	...	...
f_{81}	5.477799(25)	...	0.24, —	...	...	...	2.36(16)	...	...
f_{82}	5.484197(24)	...	0.25, —	...	...	...	5.66(15)	...	...
f_{83}	5.487352(19)	...	0.32, —	...	...	...	2.58(13)	...	...
f_{84}	5.491241(16)	...	0.39, —	...	...	...	2.90(11)	...	...
f_{85}	5.496090(20)	...	0.30, —	...	0.46, —	...	0.77(13)	...	1.24(20)
f_{86}	5.503194(26)	...	0.24, —	...	...	...	5.63(17)	...	...
f_{87}	5.510788(25)	...	0.24, —	...	...	...	4.45(17)	...	...
f_{88}	5.516547(19)	...	0.30, —	...	...	...	2.13(13)	...	...
$f_{32'}$	5.517516(25)	...	0.23, —	...	...	...	0.11(17)	...	...
f_{89}	5.522630(22)	...	0.28, —	...	...	...	5.07(15)	...	...
f_{90}	5.531191(15)	...	0.38, —	...	...	...	3.81(10)	...	...
f_{91}	5.534807(22)	...	0.27, —	...	...	...	0.56(15)	...	...
f_{92}	5.544758(22)	...	0.26, —	...	...	...	3.58(15)	...	...
f_{93}	5.593452(26)	...	0.21, —	...	...	...	3.41(18)	...	...
$2f_1$	5.61492824	4.92,+0.025	4.39,−0.008	3.89,+0.008	3.63,−0.002	4.025(23)	4.088(09)	4.124(24)	4.092(023)
f_1+f_2	5.6304667	1.83, —	1.79,−0.019	1.69,−0.008	1.30, —	5.12(07)	5.089(22)	5.19(06)	5.13(07)
f_1+f_3	5.6323002	2.99, —	2.58,+0.011	2.23,+0.023	2.34,−0.013	0.67(04)	0.647(16)	0.63(04)	0.62(04)
f_1+f_4	5.6340636	...	0.69, —	0.89, —	0.52, —	...	0.25(06)	0.36(11)	0.49(17)
f_2+f_3	5.6478387	...	0.23, —	...	...	...	1.84(17)	...	
$2f_3$	5.6496722	...	0.33, —	...	...	...	2.85(12)	...	
f_1+f_6	5.666189	...	0.18, —	...	...	...	3.65(22)	...	
$3f_1$	8.4223924	...	0.49, —	...	0.60, —	...	2.57(08)	...	2.63(14)
$2f_1+f_2$	8.4379308	...	0.21, —	...	...	...	3.44(19)	...	...
$2f_1+f_3$	8.4397643	...	0.22, —	...	...	...	5.31(18)	...	...
	N_{obs}	21251	63497	17307	18375				
	σ_A [mma]	0.12	0.04	0.09	0.09				
	$\sigma_{dA/dt}$ [mma/d]	0.012	0.003	0.010	0.009				
	Detection threshold [mma]	0.58	0.20	0.46	0.42				
	Residual SD [mma]	12.05	6.59	8.58	8.08				

3.4 Frequencies in the g-mode region

From the 2005 data, we recovered all 12 frequencies below 0.9 mHz found in the combined 2004 data (Table 2). We also detected an alias of f_G at f_{G+} in the 2005 data and think that f_{G+} is the true frequency. We also detect a dozen new frequencies in this region. We also notice that many of the amplitudes changed considerably between 2004 and 2005. While the 2004 spectrum was dominated by f_A and f_B with B amplitudes near 2.7 mma, the 2005 spectrum is dominated by f_C with an amplitude changing from ∼6 mma to ∼3 mma (Fig. 4).

The frequencies which we temporarily attribute to g-modes occur mainly between 0.1 and 0.4 mHz. However, several periodicities at higher frequencies, between 0.6 and 2.3 mHz, were also found, including f_{AA} at 2.7 mHz. Several of these were also observed in 2004 and they are most likely g-modes as well.

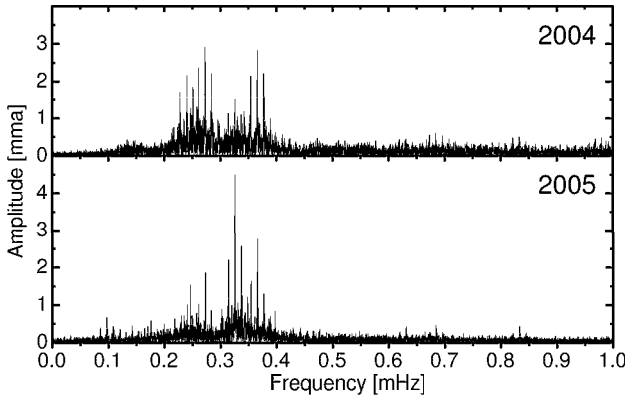

Figure 5. Fourier spectrum of Bal09 below 1 mHz for B 2004 (top) and Bvb 2005 (bottom) data.

3.5 The region of the dominant frequency (2.8 mHz)

This is the first of four narrow regions in frequency where p-modes occur. The f_1 (the highest amplitude term) has been previously identified as radial mode by Baran et al. (2008). The f_2, f_3 and f_4 form an equidistant triplet, presumably a rotationally split $\ell = 1$ mode (Bar05) and we also recovered f_5, f_6 and f_7 in this region. Additionally, two new frequencies, f_{36} and f_{37}, were found in the 2005 data. Together with f_5, f_6 and f_7 they form a nearly symmetric although not equally-spaced quintuplet which is probably an $\ell = 2$ rotationally split mode. This was partially confirmed by Baran et al. (2008) using multicolour and spectroscopic observations. In addition to the two multiplets and the radial mode we found no other frequencies in the region of 2.8 mHz except the 'ghost' terms already discussed in Section 3.3. We also noticed that the multiplet spacings changed between 2004 and 2005, becoming wider with

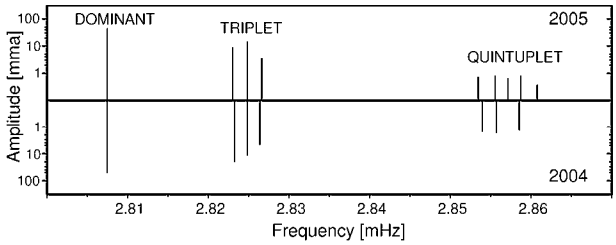

Figure 6. Schematic amplitude spectra near 2.8 mHz of 2005 (top) and 2004 data (bottom).

Table 4. Frequencies and splittings for all modes near 2.85 mHz.

#	(ℓ, m)	Frequency 2004 [mHz]	Frequency 2005 [mHz]	Difference in freq. [μHz]
f_1	(0,0)	2.8074697(02)	2.80746412(16)	−0.0056(03)
f_2	(1,+1)	2.8232390(06)	2.8230026(08)	−0.2364(10)
f_3	(1,0)	2.8248080(11)	2.8248361(06)	+0.0281(13)
f_4	(1,−1)	2.8263696(27)	2.8265995(22)	+0.2315(35)
f_5	(2,+2)	2.853958(08)	2.853383(09)	−0.575(12)
f_7	(2,+1)	2.855710(10)	2.855571(10)	−0.139(14)
f_{36}	(2,0)	—	2.857126(13)	—
f_6	(2,−1)	2.858534(14)	2.858725(10)	+0.191(17)
f_{37}	(2,−2)	—	2.860737(21)	—
Difference		Splitting 2004 [μHz]	Splitting 2005 [μHz]	Change of splitting [%]
$f_3 - f_2$		1.5690(13)	1.8336(08)	+16.86(11)
$f_4 - f_3$		1.5616(29)	1.7650(18)	+13.03(24)
$f_7 - f_5$		1.752(13)	2.188(13)	+24.9(12)
$f_{36} - f_7$		—	1.555(16)	—
$f_6 - f_{36}$		—	1.599(16)	—
$f_{37} - f_6$		—	2.012(23)	—
$f_6 - f_7$		2.824(17)	3.154(14)	+11.7(08)

time. This is shown schematically in Fig. 6. We will discuss the possible explanation of this behaviour in Section 5.

The frequencies of the multiplet components and the splittings for 2004 and 2005 are given in Table 4. We can see from this table that while the components of the triplet were within the errors equidistant in 2004, this is no longer the case in 2005 and a small assymmetry appeared. Moreover, the splittings were larger by about 15% in 2005. Not only the side components of the triplet changed their frequencies but that of the central one also changed by a significant amount. The changes of frequencies of the triplet components can be even better illustrated in the O−C diagram (Fig. 7) where nightly times of maximum light were used. For each frequency, they were obtained by subtracting all other frequencies from the Bvb data and then dividing the residuals into separate nights. Then, times of maximum brightness were derived for each night. It can be seen that while within the time interval covered by observations in each season (40–50 days), the period can be regarded as nearly constant (though different for 2004 and 2005), the changes of periods between the two seasons are evident and very large for f_2 and f_4. Unfortunately, it is not known how fast and when the periods underwent such a large change. There is an obvious ambiguity in counting pulsation cycles between 2004 and 2005

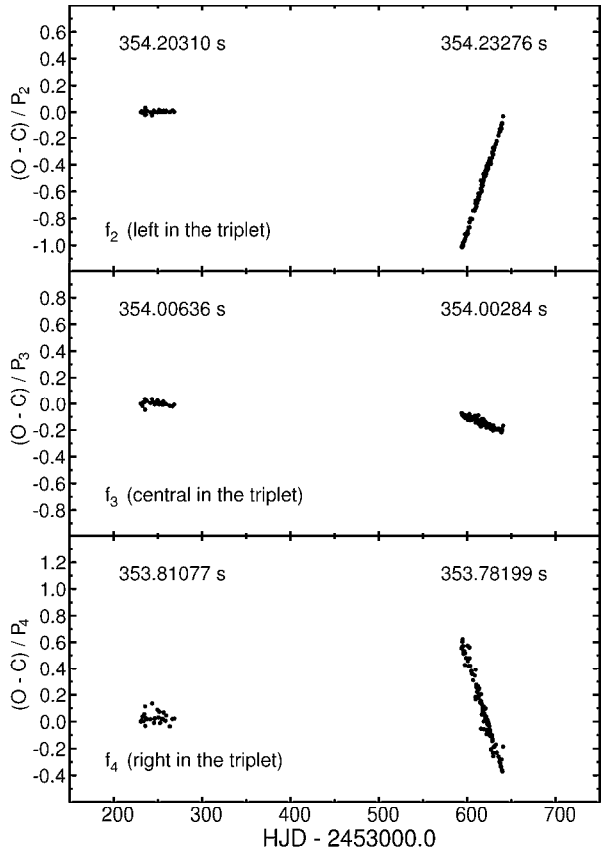

Figure 7. The O−C diagrams calculated from the nightly times of maximum light for the components of the 2.82 mHz triplet. Periods corresponding to seasonal mean values are given in the panels.

data. This means that in Fig. 7 the 2005 points could be shifted upward or downward by an integer number of pulsation cycles.

The components of the quintuplet which were detected during both 2004 and 2005 indicates that it behaves in a similar way as the triplet, i.e., increasing spacings. The change in spacings was different for the $|m| = 1$ and $|m| = 2$ components, but as a first approximation we can claim that it was proportional to $|m|$. We may therefore speculate that the same mechanism caused the change of splittings in both multiplets. It is interesting to note that the main frequency, f_1, also changed slightly between 2004 and 2005. It would be interesting to monitor this behaviour on a longer time scale as it could be used to determine evolutionary changes of the star (Reed et al. 2004).

Amplitudes have also changed for these frequencies. The largest change was observed for f_2 which decreased from 20.4 to 9.5 mma in B/Bvb data, but the amplitudes of f_1, f_4, f_5, f_6 and f_7 also decreased from 2004 to 2005. Only for f_3 did the amplitude slightly increase.

3.6 Other regions with p-modes

There are three other frequency regions where p-modes occur, namely at 3.8 mHz, 4.7 mHz and 5.5 mHz. These regions contain frequencies with very small amplitudes. Most of them were detected only in the Bvb data and very few of these were found in the 2004 data. Of the frequencies from 2004 that were recovered in the 2005 data, they typically had smaller amplitudes, f_8 being an example. A proper correlation of the 2004 frequencies to those

in the 2005 data has three complications: (i) The presence of many frequencies with similarly small amplitudes; (ii) strong aliasing; and (iii) frequencies corresponding to $|m| > 0$ modes might have changed their frequencies considerably between 2004 and 2005, as seen in the multiplets. These uncertainties lead to ambiguities in frequency correlation which are indicated in Table 3 using double identifications and question marks.

As the frequency densities are high within each region, some of the frequencies are likely members of rotationally split multiplets. However, ℓ and m mode assignment would be uncertain from our data. Nevertheless, their frequencies may be useful for asteroseismology once the character of long-term frequency-spacing changes is established. It is also possible that other, currently undetected components of multiplets will be detected in future observations allowing the full structure of multiplets to be observed. These regions are therefore potentially very important for future asteroseismological analyses.

There is also an isolated frequency (f_{38}) near 3.036 mHz, which is between p-mode regions. Its amplitude is very small but its detection has been confirmed by G. Fontaine (private communication) in an independent set of data, and so we consider it to be intrinsic to Bal09.

3.7 Combination frequencies

From the 2005 data, 17 combination terms were detected in five distinct regions. They are typically a simple sum or difference of two frequencies. Of them, the most important are those that involve g- and p-modes as it proves that both kinds of modes occur in the same star. They were previously detected by Bar05 and are detected in the combined 2004 data. There are six g- and p-mode combination frequencies observed in the 2005 data and three in the 2004 data. We do not recover the $f_8 - f_1$ and $f_1 + f_8$ combinations present in the 2004 data (Table 2), but we do detect combination frequencies in two new regions: sums of g- and p-modes and $2f_1 - f_3$. We also detect two harmonics of f_1. Their amplitudes and phases indicate that despite a decrease of the B-filter amplitude by about 14% between 2004 and 2005, the shape of the light curve of the main mode remained practically unchanged.

3.8 Remarks on the frequency spectrum

Before we try comparing observed frequencies with those derived from stellar models, a few general comments on the frequency spectrum need to be made. The substantial data sets of 2004 and 2005 indicate undoubtedly that amplitude variations are very common in this star. Some amplitudes changed by a factor of 2–3 over the span of our data. Figure 4 indicates that the time scale of amplitude changes might be as short as two weeks. Amplitude changes were also observed in other sdBV stars. For example, Kilkenny et al. (2006) present the results for four sdBV stars which have been observed at least twice. Their analysis showed that for three of them the amplitudes of some modes have changed significantly. For example, for EC 20338−1925 the dominant mode decreased its amplitude from 26 to 4 mmag. A similar change was found for V 338 Ser. Amplitude changes have also been observed in other sdBV stars. (Reed et al. 2007b) examined follow-up data on 23 sdBV stars (including some Bal09 data) and of 54 consistently detected frequencies, 34 (63%) changed amplitudes by more than a factor of two over the duration of their observations. Fourteen of their frequencies changed amplitudes by more than a factor of five; including one that ranged from 57 to 8 mma. Therefore, the amplitude variations in Bal09 are consistent with those observed in many other sdBV stars.

We also detect a clear change of frequencies, especially of those known to have $|m| \neq 0$, i.e., the side components of the rotationally split multiplets. A small frequency change of the radial mode f_1 was also detected. It would be interesting to trace these changes during a longer time scale, not only in Bal09, but also in other sdBV stars. They can be used to constrain the evolution of sdB stars and/or indicate the mechanism that causes these changes.

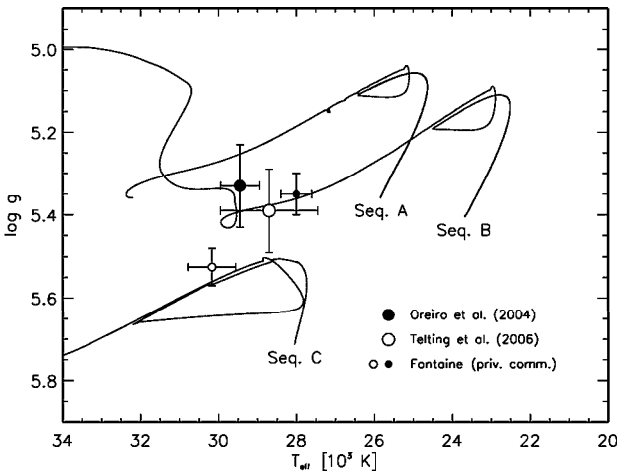

Figure 8. Physical parameters for Bal 09 derived by different authors. Three sdB evolutionary sequences (A, B, C) used for theoretical comparison are also shown.

4 COMPARISON WITH THEORETICAL FREQUENCIES

4.1 The models

Once the observed frequencies have been determined, it is interesting to compare them with theoretical frequencies computed for models of sdB stars. For this purpose, we computed three sdB evolutionary sequences (A, B, C). These sequences begin at the onset of He-core burning and their parameters are given in Table 5, while the evolutionary tracks are shown in the $T_{\rm eff}$ – $\log g$ diagram of Fig. 8. For comparison, four spectroscopic determinations of $T_{\rm eff}$ and $\log g$ of Bal09 are also shown with error bars. They were taken from Oreiro et al. (2004), Telting et al. (2006), and Fontaine (private communication).

Sequences B and C were obtained by evolving an 1 $M_\odot$ star from the main sequence using the stellar evolution code of Jimenez & MacDonald (1996). A different mass loss Reimer's parameter on the red giant branch leads to sdB tracks with different H-envelope mass ($M_{\rm H}$), althought with very similar total mass ($\sim$0.47 $M_\odot$), as the core needed to ignite He-core burning is almost the same in all cases. No binary mass transfer was included. The position of an evolutionary sequence in the $T_{\rm eff} - \log g$ plane depends mainly on the total mass (M) and on $M_{\rm H}$. Tracks with the same M locate along a diagonal in this plane, ordered by $M_{\rm H}$: the lower $M_{\rm H}$, the larger $T_{\rm eff}$ and $\log g$ are. The diagonal is shifted to higher (lower) temperatures if M is increased (reduced). Thus, comparing the spectroscopic parameters of Bal09 with the location of sequences B and C (Fig. 8), we may conclude that either the star is at the final stages of He-core burning (or past it) or it is at the beginning of the

Table 5. Parameters of stars at the beginning of the He-core burning phase for three evolutionary sequences. Provided are total mass (M), H-envelope mass ($M_{\rm H}$), effective temperature ($T_{\rm eff}$) and logarithm of surface gravity ($\log g$).

Model	M $[M_\odot]$	$M_{\rm H}$ $[M_\odot]$	$T_{\rm eff}$ [K]	$\log g$ [dex]
A	0.554	$2.9{\cdot}10^{-3}$	25 860	5.36
B	0.475	$3.1{\cdot}10^{-3}$	23 690	5.40
C	0.473	$4.6{\cdot}10^{-4}$	28 060	5.71

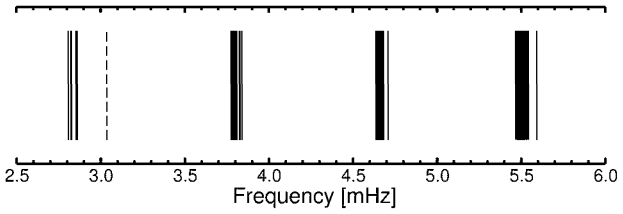

Figure 9. Schematic frequency spectrum of Bal 09 in the region where the likely p modes occur. Dashed line corresponds to f_{38}.

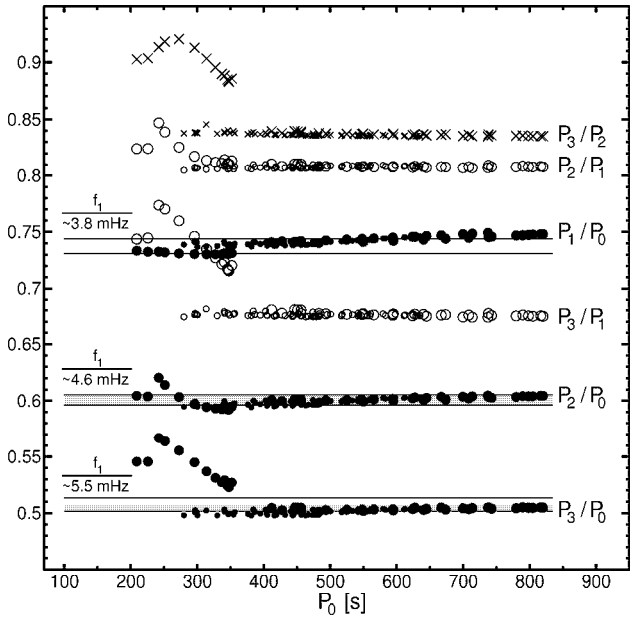

Figure 10. Period ratios for the first four radial orders of radial modes plotted as a function of the period of the fundamental radial mode, P_0. Two sets of models were used: (i) those described in Section 4.1 and listed in Table 5 (large symbols), (ii) the sequences 5 to 7 from Charpinet et al. (2002) (small symbols). Three horizontal strips denote the observed ranges of frequency ratios. All modes from p-mode groups near 3.8, 4.7 and 5.5 mHz are considered.

sdB phase, but with a total mass higher than 0.47 $M_\odot$. In the latter case, formation channels involving binary interaction should be included to account for the higher mass. To allow for the posibility of higher mass for Bal09, a third evolutionary sequence (A) was computed ad hoc with a slightly higher total mass (0.55 $M_\odot$) than for sequences B and C. Its parameters at He-core ignition are also included in Table 5.

4.2 Analysis of p-modes

In Fig. 9 a schematic spectrum of Bal 09 in the p-mode domain is presented. As can be seen, all p-modes but f_{38} cluster in four narrow (from 0.05 to 0.12 mHz wide) frequency groups near 2.8, 3.8, 4.7 and 5.5 mHz, consisting of 9, 22, 24, and 16 frequencies, respectively (Table 3).

Using combined multicolour photometry and spectroscopy of Bal09, Baran et al. (2008) identified f_1 as a radial mode and constrained the ℓ value for the 2.825 mHz triplet components and f_8. For a complete identification of f_1, its radial order (n) needs to be determined. Assuming that f_1 is the fundamental radial mode (ℓ = 0, n = 1) and using the grid of sdB models of Charpinet et al. (2002), Bar05 came to a reasonably good agreement between the observed frequency and the location of Bal09 in the $\log g - \log T_{\rm eff}$ diagram (see Fig. 13 in Bar05). The first overtone was not regarded as an alternative for f_1 by Bar05, however. Let us consider such a case. The period of this fundamental radial mode (P_0) would be of the order of 356 s/0.74 $\approx$ 480 s, which is not detected in our data sets.[1] Model periods can be matched within the spectroscopic $\log g$ and $T_{\rm eff}$ constraints only if slightly more massive models than those of Charpinet et al. (2002) are considered, e.g. some models on sequence A in Fig. 8. We can also find an appropriate model if we assume that f_1 is the second radial overtone, though the match is worse. In this case P_0 equals to 593 s. However, all models of a given P_0 have nearly the same value of $\log g$. This can be explained as the period of the fundamental radial mode depends primarily on average density, i.e., stellar radius. For a set of models that do not differ very much in mass this implies that models with the same pulsation period would have approximately the same $\log g$. This can be seen, for example, in the bottom panel of Fig. 13 of Bar05. As the spectroscopic error box for $\log g$ and $T_{\rm eff}$ is still quite large (Fig. 8) we cannot constrain n for f_1 since both the fundamental and first overtone are allowable, and even the second overtone cannot be excluded. While only higher overtones can be rejected, we can constrain $\log g$ for our three possibilities to 5.51 (f_1 fundamental), 5.34 (1st overtone), or 5.22 (2nd overtone). Improved constraints on $\log g$ will distinguish between these three possibilities. We prefer to assume that f_1 is the fundamental radial pulsation as this is the most likely possibility. If f_1 were the first overtone then the fundamental radial pulsation (and also some non-radial p modes with similar frequencies) should occur near 2.1 mHz and these pulsations are not observed.

Another argument in favour of f_1 as the fundamental radial mode is the overtone ratio. If we assume that at least one mode in the 3.8 mHz group is also radial then the overtone ratio is 2.807 mHz/(3.774 $\div$ 3.841) mHz $\approx$ 0.731 $\div$ 0.744 which can be compared with theoretical ratios, as is done in Fig. 10. It can be seen that for most models the P_1/P_0 ratio is near to 0.7 and only for model C is P_3/P_1 also allowed. The latter case implies f_1 to be the first overtone. As such, we can conclude that if any of the 3.8 mHz-region frequencies are radial, then f_1 is most likely the fundamental radial pulsation. Additionally, Fig. 10 indicates that by choosing f_1 to be the fundamental radial mode, the 4.7 mHz and 5.5 mHz groups match overtone ratios for P_2/P_0 and P_3/P_0. It seems unlikely that such a good match is serendipitous. Reversing this reasoning we may therefore conclude that each of the groups of p-modes in Bal09 may contain a radial mode (if so, we know which overtone it is). Alternatively, the same could be true for consecutive

[1] 0.74 is the period ratio of the first overtone and fundamental radial modes (P_1/P_0) found from theoretical models; see also Fig. 10.

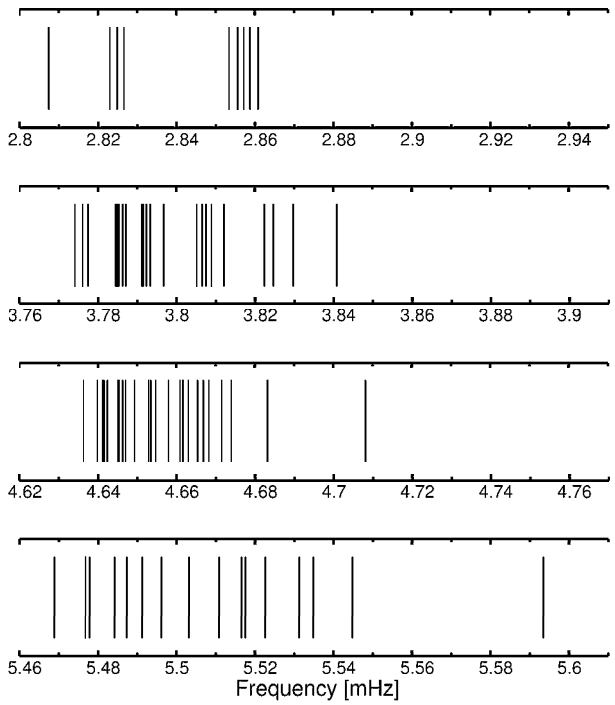

Figure 11. A schematic frequency pattern in four groups of p modes: near 2.8, 3.8, 4.7, and 5.5 mHz.

overtones of non-radial modes as some of these have period ratios similar to the radial ones.

Using the previously discussed multiplets, we can search for additional multiplets using the same frequency spacing. Additional multiplets can be used to identify modes. Because of the high frequency density in these regions, there are likely rotationally split multiplets. However, the simple structure of frequencies in the 2.8 mHz group contrasts with more complicated frequency patterns in the three remaining groups of p-mode frequencies (Fig. 11). Another likely multiplet is the symmetric triplet of f_{72}, f_{73}, and f_{74} (Table 3) with splittings of 1.440 ± 0.021 and 1.446 ± 0.023 μHz. Bearing in mind the richness of the spectrum, observed amplitude variations, and uncertainties caused by aliasing, we prefer not to speculate further on additional multiplets until better data more fully reveal the frequency spectrum. The high frequency density also indicates that all groups of p-modes must have $\ell > 2$ modes, except those in the 2.8 mHz region.

4.3 Analysis of g-modes

Bal 09 shows a very rich spectrum in the low-frequency domain, which theoretically corresponds to g-modes. In Fig. 12, the schematic amplitude spectrum of Bal 09 in this frequency range is displayed. For comparison, theoretical frequencies of a representative sdB model in sequence C are also shown. We did not intend to find a model which matches the observed frequencies; the theoretical frequencies are shown just to compare the density of theoretical and observed frequencies in this region. As can be seen in Fig. 12, at least $\ell = 1$ and 2 modes are needed to account for the observed frequencies. However, as the density of theoretical frequencies increases with ℓ, the observed spectrum would be better reproduced if higher degree modes were considered.

We also notice a lack of frequencies between 0.4 and 0.6 mHz. Either they have amplitudes below our detection threshold or they

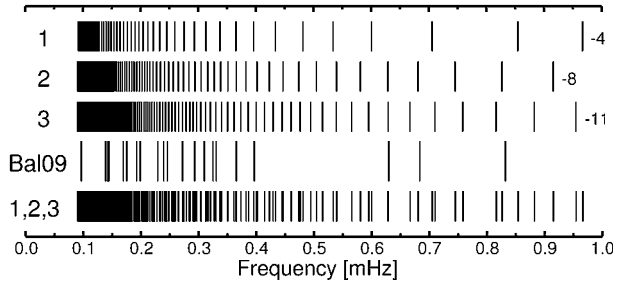

Figure 12. Schematic frequency spectrum of Bal 09 below 1 mHz compared with theoretical ones for g-modes with $\ell = 1$, 2 and 3 (shown on the left). The latter are shown for a representative sdB model from sequence C. Numbers on the right indicate the value of n for the first g mode below 1 mHz.

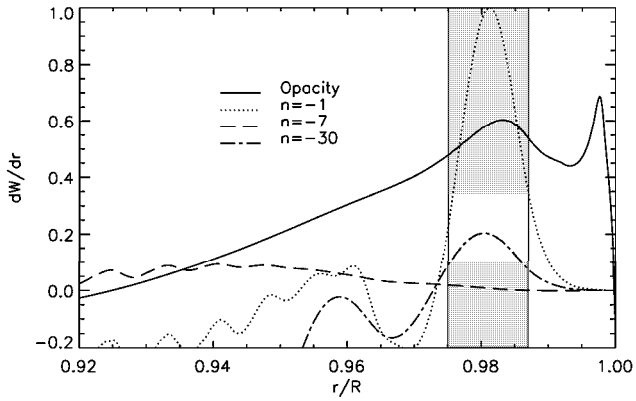

Figure 13. Derivative of the work integral for $\ell = 2$, $n = -1$, -7, and -30 g-modes as a function of a fractional stellar radius for a representative model from sequence C. Regions contributing to driving (damping) produce positive (negative) dW/dr values. The Rosseland mean opacity is included as a solid line and plotted in arbitrary units. Vertical lines delimit the driving region (gray) associated with an iron-group opacity bump.

are not excited. We investigate the possibility that they are not excited and show the derivative of the work integral (dW/dr) for model g-modes with $\ell = 2$ and radial orders $|n| = 1$, 7 and 30 in Fig. 13. There were chosen as they are representative of low, intermediate and high radial orders. We used the GRACO non-adiabatic code (Moya et al. 2006) to compute dW/dr which is positive in regions contributing to driving oscillations, while negative in damping regions. For hot B subdwarfs the driving zone is related to the iron-peak elements opacity bump. In Fig. 13, the Rosseland mean opacity of each model is plotted as solid lines and the dotted vertical lines indicate the region of the opacity bump. Fig. 13 shows that, while the region of the bump (shown in gray) contributes to the excitation of low- and high-radial order modes ($dW/dr > 0$ there), it has a negligible effect in driving intermediate-radial order modes. This result could support the hypothesis that g-modes with intermediate radial orders are not excited in Bal 09. Non-adiabatic computations by Jeffery & Saio (2006) also result in exciting low- and high-order g-modes but damping intermediate ones for some models. This seems a reasonable explanation for the lack of observed frequencies between 0.4 and 0.6 mHz. Model g-modes with low radial orders can have frequencies up to ~2.3 mHz (not shown in Fig. 12). We detect three frequencies (f_X, f_Y and f_Z) between 1.8 and 2.3 mHz which could be low radial order g-modes.

Most g-modes observed have periods in the range between

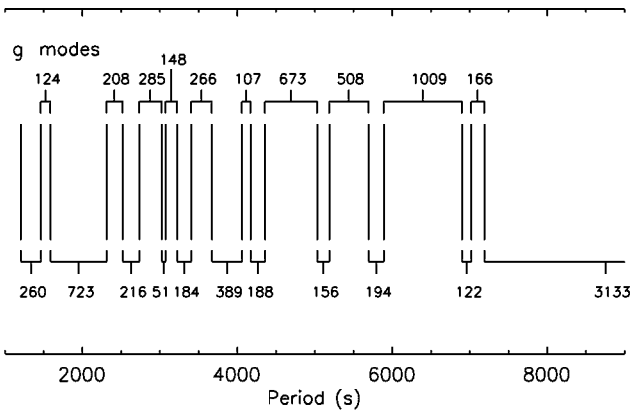

Figure 14. Schematic g-mode spectrum *in periods* of Bal 09. Period distances between adjacent modes are indicated with numbers expressed in seconds.

2500 and 7200 s, although a few extend this range to 1200–10300 s. Model g-modes with ℓ = 1–3 and periods in the range 2500–7200 s (Fig. 12) have radial orders in the range $|n| \sim$11–80, which extends to $|n| \sim$ = 5–115, if we include all of the observed periods. With high-radial orders, we can expect asymptotic behaviour which results in equally-spaced periods (Tassoul 1980). However, Charpinet et al. (2000a) have shown that sdBs might display trapped g-modes, mainly caused by the chemical transition between the He and H radiative layers in the envelope. Mode trapping causes some periods to move away from asymptotic behaviour. In Fig. 14, we show a schematic g-mode spectrum *in periods* and indicate the differences (in seconds) between adjacent periods. However, the observed period spectrum does not appear equally spaced, which suggests that some n orders were not detected or excited. Fig. 12 also shows that the density of theoretical periods is much higher than the observed density, even if only periods with $\ell \leqslant 3$ are considered.

We searched for equally-spaced periods using different techniques. While we could produce some reasonable alignments in echelle diagrams (e.g. for period spacing $\Delta P \sim 286$ s), the results are not convincing. If mode trapping is effective, we should not expect good alignment from an echelle diagram. A way around this problem would be to fine-tune models using the p-modes and then search the g-modes for periodicities, or even match their periods directly to the model ones. If some g-modes could be identified, it could greatly increase our understanding of sdB interiors.

5 DISCUSSION AND CONCLUSIONS

The 2005 campaign on Bal09 occured because it is one of the most interesting pulsating sdB stars. It has high-amplitude oscillations, it is one of the brightest sdB pulsators (B = 11.8 mag), and it has the richest pulsation spectrum of both p- and g-modes. The 2005 campaign led to the discovery of nearly a hundred independent frequencies (Table 3). Moreover, we showed that, like in many other sdBV stars (Reed et al. 2007b), amplitudes of many modes in Bal09 vary and the time scale of these changes is as short as several weeks. The 2005 data also allowed the detection of all components of the quintuplet. This was possible because of the low detection threshold of $\sim$0.2 mma in the Bvb data. The low detection threshold resulted in the detection of a large number of frequencies, especially near 3.8 and 4.7 mHz. Even if some of them turn out to be non-axisymmetric multiplets, the frequency density is such that at least some of them must have $\ell > 2$. The most surprising result of this campaign is the discovery of a considerable change of splittings in two multiplets (a triplet and quintuplet) which are believed to be rotationally split ℓ = 1 and 2 modes. As far as we are aware, this is the first clear detection of such a change of splitting in any pulsating star. The possible reasons for the change are briefly discussed below.

These results indicate that Bal09 may be a key object in our understanding of pulsations in sdBV stars and its variability is definitely worth further study. First, the changes of splittings should be monitored on a longer time scale as this may help to understand their origin. The same is true for amplitude changes. Next, as the amplitudes change so distinctly, it may happen that modes undetectable in one season will become visible in the other, thus allowing to a complete spectrum of excited modes. Finally, the observed frequencies should be compared to a larger grid of models using identifications of the strongest frequencies as done in Baran et al. (2008). Such constrained modes should result in constraining global stellar parameters for Bal09 and reveal its internal structure.

The presence of multiplets is usually attributed to rotation of the star, causing the m degeneracy to be broken. Two clear multiplets are detected in Bal 09: an ℓ = 1 triplet at 2.82 mHz and an ℓ = 2 quintuplet at 2.85 mHz. The structure of the quintuplet is specially interesting. Its components, all of which are detected in 2005, form a symmetric but not equidistant pattern. Specifically, the mean splitting between $|m|$ = 2 and $|m|$ = 1 components (2.100 $\pm$ 0.014 μHz) is considerably larger than the mean splitting between $|m|$ = 1 component and the central peak of the quintuplet (1.577 $\pm$ 0.007 μHz). The same was true in 2004. Such a pattern cannot be produced by a solid body rotation, nor even by a spherically symmetric rotation, $\Omega = \Omega(r)$. Indeed, in both these cases splitting within a multiplet is, in the limit of slow rotation, proportional to m (e.g. Kawaler & Hostler 2005). Consequently, components of the multiplet have to be equidistant. This is not what we see. Thus, the observed structure of ℓ = 2 quintuplet implies that rotation rate of Bal 09 must depend on the stellar latitude, θ.

Additional information can be inferred from comparison of rotational splitting for $|m|$ = 2 and for $|m|$ = 1. Because of its spacial structure, modes of $|m|$ = 2 are most sensitive to equatorial rotation of the star, while modes of $|m|$ = 1 sense mostly rotation in the intermediate latitudes. The observed splitting is larger for $|m|$ = 2, which implies that rotation of Bal 09 is fastest on the equator. This has to be true at least in the large part of the star's envelope. Qualitatively, this dependence on θ is similar to that observed in the Sun (e.g. Thompson et al. 2003).

The most puzzling result of 2005 campaign is detection of changing rotational splittings. Both in the triplet and in the quintuplet the separation of components is much wider in 2005 than in 2004. The differences range from 12% for ℓ = 2 $|m|$ = 1 to 16% for ℓ = 2 $|m|$ = 2. Similar behaviour of both multiplets puts strong constraint on any theoretical explanation of the observed effect. For example, it excludes internal 1:1 resonances within the multiplets (Buchler et al. 1995). Such a coupling could modulate the separation of multiplet compenents, but it would act in each multiplet independently, giving no explanation why they all change in the same way. Simultaneous widening of both multiplets must be caused by a common mechanism, which affects structure of the star.

Taken at the face value, widening of multiplets in Bal 09 would imply a considerable change of its internal rotation, occurring in just one year. At first glance this seems to be a very far fetched hypothesis. However, variations of internal stellar rotation on time scale of a few years are not unheard of. Such variations are actually observed in the Sun (Shibahashi 2004; Howe 2008). These

so-called torsional oscillations cause periodic changes of the solar rotation pattern with the 11-year solar cycle.

The cause of torsional oscillations in the Sun is not clear, although several hypotheses have been put forward (Shibahashi 2004). We must note that internal structure of Bal 09 and of the Sun is very different. In contrast to the Sun, the envelope of an sdB star is almost entirely radiative, with the exception of an extremely thin convective layer associated with the He II ionisation zone (Charpinet et al. 2000b). However, the presence of convection is not necessary to drive torsional oscillations in the star. They can be excited by interaction between differential rotation and magnetic field (Goode & Dziembowski 1991). In this mechanism, differential rotation and the toroidal component of the field exchange energy, causing periodic redistribution of angular momentum inside the star. This in turn, leads to periodic changes of rotational splittings. According to Kawaler & Hostler (2005), strong differential rotation is what we expect in envelope of every sdB star. The magnetic field in Bal 09 has not yet been measured, but observations of several other sdB stars reveal fields of $\sim$1.5 kG (O'Toole et al. 2005). The amplitude of torsional oscillations discovered in the Sun is rather small, of the order of 1 – 1.5% of the local rotation velocity. This is way too small to account for changes in multiplet splittings as large as those observed in Bal 09. Torsional oscillations in Bal 09 have to be at least an order of magnitude stronger than in the Sun. Whether torsional oscillations in Bal 09 can be driven to such amplitudes remains an open question until detailed model calculations become available.

ACKNOWLEDGMENTS

This project was partially supported by grant no. 1P03D 013 29 kindly provided by Polish MNiSW. AB acknowledges help of students of University of Hawaii at Hilo: A. Hackmann, J. Berghuis, H. Butler, T. Shimura, M. Hyogo, B. DeKoning, and J. Slivkoff during his observations at Mauna Kea. MDR and AYZ were supported by the National Science Foundation Grant AST007480. Any opinions, findings, and conclusions or recommendations expressed in this material are those of the author(s) and do not necessarily reflect the views of the National Science Foundation. Travel grants for MDR were supplied by the American Astronomical Association.

REFERENCES

Baran A., Pigulski A., Kozieł D. et al., 2005, MNRAS, 360, 737
Baran A., Oreiro R., Pigulski A. et al., 2006, BaltA, 15, 227
Baran A., Oreiro R., Pigulski A. et al., 2007, A.S.P. Conf. Ser., 372, 607
Baran A., Pigulski A., O'Toole S.J., 2008, MNRAS, 385, 255
Bixler J.V., Bowyer S., Laget M., 1991, A&A, 250, 370
Buchler J.R., Goupil M.-J., Serre T., 1995, A&A, 296, 405
Charpinet S., Fontaine G., Brassard P. et al., 1997, ApJ, 483, L123
Charpinet S., Fontaine G., Brassard P. et al., 2000a, ApJS, 131, 22
Charpinet S., Fontaine G., Brassard P., Dorman B., 2000b, ApJS, 131, 223
Charpinet S., Fontaine G., Brassard P., Dorman B., 2002, ApJS, 140, 469
Downes R.A., 1986, ApJS, 61, 569
Fontaine G., Brassard P., Charpinet S. et al., 2003, ApJ, 597, 518
Goode P.R. & Dziembowski W.A., 1991, Nature, 349, 223
Green R.F., Schmidt M., Liebert J., 1986, ApJS, 61, 305
Green E.M., Fontaine G., Reed M.D. et al., 2003, ApJ, 583, L31
Howe R., 2008, AdvSpRes, 41, 846
Jeffery C.S. & Saio H., 2006, MNRAS, 372, L48
Jimenez R. & MacDonald J., 1996, MNRAS, 283, 721
Kawaler S.D. & Hostler S.R., 2005, ApJ, 621, 432
Kilkenny D., Koen C., O'Donoghue D. et al., 1997, MNRAS, 285, 640
Kilkenny D., Kotze J.P., Jurua E., Browstone M., Babiker H.A., 2006, BaltA, 15, 255
Moya A., Garrido R. & Dupret M.A., 2004, A&A, 414, 108
O'Donoghue D., Lynas-Gray A.E., Kilkenny D., Stobie R.S., Koen C., 1997, MNRAS, 285, 657
Oreiro R., Ulla A., Pérez Hernández F. et al., 2004, A&A, 418, 243
Oreiro R., Pérez Hernández F., Ulla A. et al., 2005, A&A, 438, 257
Østensen R.H., 2000, Ph. D. thesis, University of Tromsø, Norway
O'Toole S.J., Jordan S., Friedrich S., Heber U., 2005, A&A, 437, 227
Reed M.D., Kawaler S.D., Zoła S., et al., 2004, MNRAS, 348, 1164
Reed M.D., O'Toole S.J., Terndrup D.M., et al., 2007a, ApJ, 664, 518
Reed M.D., Terndrup D.M., Zhou A.-Y., Unterborn C.T., An D., Eggen J.R., 2007b, MNRAS, 378, 1049
Schuh S., Huber J., Dreizler S. et al., 2006, A&A, 445, 31
Shibahashi H., 2004, IAU Symp. 223, 23
Silvotti R., Schuh S., Janulis R. et al., 2007, Nature, 449, 189
Stetson, P.B., 1987, PASP, 99, 191
Stetson, P.B., 1990, PASP, 102, 932
Stobie R.S., Kilkenny D., O'Donoghue D. et al., 1997, MNRAS, 287, 848
Tassoul M., 1980, ApJS, 43, 469
Telting J.H., Østensen R.H., Heber U., Augusteijn T., 2006, BaltA, 15, 235
Thompson M.J., Christensen-Dalsgaard J., Miesch M.S., Toomre J., 2003, ARAA, 41, 599